

Original Research Article

Development of an additively manufactured head and neck phantom for computed tomography studies

M. Wegner^{1,2*}, N. Hinrichsen¹, M. Rosendahl², D. Krause¹, and E. Gargioni²

¹ Institute of Product Development and Mechanical Engineering Design, Hamburg University of Technology, Hamburg, Germany

² Department of Radiotherapy and Radiation Oncology, University Medical Center Hamburg-Eppendorf, Hamburg, Germany

* Corresponding author, email: marie.wegner@tuhh.de

© 2025 Marie Wegner; licensee Infinite Science Publishing

This is an Open Access abstract distributed under the terms of the Creative Commons Attribution License, which permits unrestricted use, distribution, and reproduction in any medium, provided the original work is properly cited (<http://creativecommons.org/licenses/by/4.0>).

Abstract: Additive manufacturing offers significant potential for the design of medical phantoms used in quality assurance for medical imaging and treatment planning. This study presents the design and fabrication of a head and neck phantom for computed tomography (CT) quality assurance. Appropriate infill densities of polylactic acid were selected to achieve tissue-equivalent CT values, enabling the integration of many anatomical structures in the head and neck region. A bone surrogate material was incorporated post-processing to achieve high density values that are unachievable with common 3D printing materials. CT validation confirmed the phantom's ability to replicate the appropriate Hounsfield unit, demonstrating its suitability for imaging-based assessments. This phantom provides a reproducible and customizable solution for treatment verification in head and neck cancer therapies.

I. Introduction

Head and neck cancer (HNC) contributes significantly to cancer-related mortality worldwide [1]. The rising numbers are partly due, on the one end, to an increased spread of the human papillomavirus (HPV) infection and, on the other hand, due to continued high levels of alcohol and tobacco consumption [1, 2]. HNC tumors are often small and highly heterogeneous, making accurate diagnosis and effective treatment particularly challenging. Advanced imaging techniques play a crucial role in identifying and characterizing these tumors, yet limitations in standardization and validation still hinder their full clinical potential.

Radiomics, an emerging field that utilizes artificial intelligence to extract and analyze quantitative features from radiological images, like computer tomography (CT) images, offers promising prospects for predicting tumor control and, possibly, adapting therapy. In fact, by identifying subtle patterns and correlations between imaging data and clinical outcomes, radiomics has the potential to enhance diagnostic and treatment precision. However, despite its potential, radiomics remains an

evolving field with significant challenges, including the lack of standardized methodologies and validated protocols for clinical implementation.

Commercial head phantoms are typically generic and homogeneous, representing only bones, teeth, and surrounding soft tissue. This limitation is also present in existing additively manufactured (AM) head phantoms found in the literature [3–7], as they do not differentiate between soft tissue structures and individual organs. While one study presents a full head phantom [3], the others focus on head slices [4–7], further limiting anatomical representation. Additionally, CT-appropriate skull models have been explored in the literature [8, 9], but these primarily focus on improved representation of bone structures. These head phantoms are fabricated using direct or indirect AM manufacturing methods [10], with a high potential for tissue mimicking. The integration of all anatomically relevant details for HNC applications, however, still remains unaddressed.

The aim of this study is, therefore, to develop and validate a physical patient-specific head and neck phantom designed for CT imaging, specifically for the study of

HNC. This phantom should provide a controlled environment to investigate radiomic features while allowing systematic variation of CT scanners, acquisition techniques, and reconstruction parameters using the same “patient”. Additionally, the phantom will serve as a valuable tool for quality assurance in imaging protocols and can be utilized for future dose measurement studies, ultimately contributing to the optimization of CT imaging techniques for head and neck oncology.

II. Material and methods

We developed the head and neck phantom using the methodological workflow for additive manufactured phantoms presented in Wegner and Krause [11], which structures the development into four phases: (i) phantom planning, (ii) concept definition, (iii) phantom design, and (iv) phantom validation. While the first three phases are described in this section, the validation of the phantom is part of the results section.

II.I. Phantom planning

During the first phase, we established the list of requirements together with the stakeholders involved. To gather the requirements, we used the online-based phantom requirements survey by Wegner et al. [12]. This survey addresses the phantom classification characteristics, like type, purpose, area of application and anatomy, as well as desired custom design characteristics. The head and neck phantom needs to be a physical phantom for quality analysis in CT-imaging. The geometrical design is supposed to be anthropomorphic, including head and neck organs that are relevant for HNC radiotherapy treatment. In particular, we are interested in radiation-sensitive organs and structures, whose imaging properties, based on radiomics, could vary during treatment. A physical parameter that can be measured for these organs/structures in CT imaging is the x-ray attenuation, in terms of CT numbers in Hounsfield units (HU). These properties need to be mapped into the phantom, based on patient and literature data. Moreover, an important phantom requirement is that the shape of these internal structures represents the actual patient anatomy with a high level of similarity.

II.II. Concept definition

In the concept phase the focus was the determination of suitable tissue-mimicking CT materials. To evaluate possible additive manufactured materials, we previously performed several tests for different Fused Deposition Modelling (FDM) materials and infills, using simple cone-shaped geometries [13]. Based on this evaluation at the material level, the results were implemented into the CT representation of anatomical structures in the phantom.

For the skeletal bone, we investigated different mixtures as surrogate material. In particular, we used silicone (Shore 0), and silicon oil with additives of varying concentrations

of gypsum, strontium carbonate (SrCO_3) and calcium carbonate (CaCO_3).

Additionally, we evaluated the visibility of glue, employed for safe attaching of PLA components in CT scans and its potential impact on measured CT numbers HU. The analysis revealed that, due to the small adhesive surface, neither the glue nor the connection between individual segments was distinguishable in the CT images.

II.III. Phantom design and manufacturing

To generate a patient-specific model of the head and neck region, we selected a patient from the online database *HaN-Seg: The Head and Neck Organ-at-Risk CT & MR Segmentation Dataset* [14, 15]. This database provides organ-at-risk segmentations for the head and neck region of 42 patients. The selection criteria for the patient were (i) complete anatomy (including teeth, ideally without metal fillings), (ii) a closed mouth, (iii) a CT scan with good resolution and (iv) no hyper-extended position of the patient. The patient-specific segmented data are necessary to generate a 3D model as a base for the phantom.

The organs and structures that we considered from the segmentations were: the cervical esophagus, cricopharyngeal inlet, larynx, lips, oral cavity, parotid gland, pituitary gland, spinal cord, thyroid gland, lens, and vitreous body. Moreover, we manually segmented the brain, skeleton, body, cerebrospinal fluid (liquor) and teeth using *3D Slicer* [16]. All organs were exported as STL files using *3D Slicer* and further processed in *Autodesk Meshmixer* and *Autodesk Fusion* (Autodesk, Inc., San Rafael, CA, United States) to create smooth, defect-free models. The bone structures of the skeleton, skull, as well as the teeth, were entirely subtracted from the body, leaving a hollow cavity for later filling. The organs are displayed in Fig. 1.

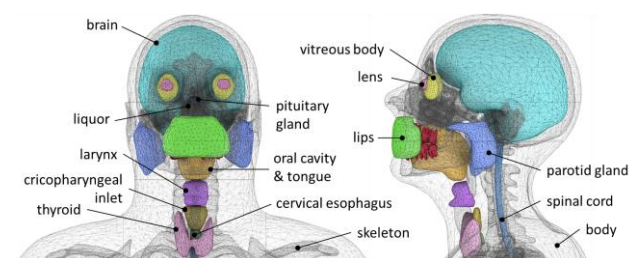


Figure 1: Internal organs within the phantom. Front view (left), side view (right).

To enable AM of the head and neck phantom, the phantom was divided into ten sections. This division was necessary due to the build volume limitations of the FDM printer. Additionally, the creation of sub-volumes facilitates access for filling the bone structures. The sections, shown in Fig. 2, include: skull cap, eyes, oral cavity (bottom and top), larynx, neck, and shoulders (right and left, separately). Additionally, the brain (which includes the pituitary gland

and the liquor), as well as the teeth, were manufactured separately (Fig. 2).

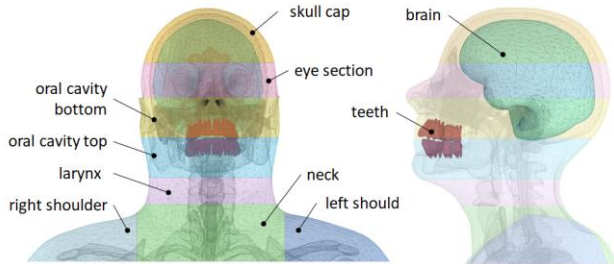


Figure 2: Sections (sub-volumes) of the phantom. Front view without the brain (left), side view including brain and teeth (right).

We prepared AM in Cura (Ultimaker B.V., Geldermalsen, The Netherlands) and printed the sections mentioned above using white PLA (Das Filament, Braunschweig, Germany) with the FDM printer *Ultimaker S5* (Ultimaker B.V., Geldermalsen, The Netherlands), with a 2.85 mm filament thickness, 0.15-layer height, and 0.4 extrusion width (see Fig. 3). The chosen line infill densities for the different organs are listed in Table 1. The percentages of infill densities were derived from a linear regression of the analysed PLA in our previous material study [13].

For manufacturing the teeth an LCD Anycubic Photon M3 printer (Anycubic, Shenzhen, China) was used. To the Engineering LCD Resin Flex 63A (FormFutura, Nijmegen, The Netherlands) strontium carbonate (45% wt.) was added before printing. Following the printing process, the support structures were manually removed, and the teeth were positioned into their designated sections in the upper and lower jaw, as illustrated in Fig. 3.



Figure 3: Additive Manufacturing of the head and neck phantom components, during FDM printing (left), teeth with support structure (top right), segment of the oral cavity with teeth (bottom right).

For the bone silicon (RTV, Shore 0, by Silikonfabrik, Ahrensburg, Germany) was thoroughly mixed with

strontium carbonate (12% wt.) and poured into the empty bone cavities, which were accessible through the segments. Only one additional opening on the skull cap top was needed for pouring. This opening was closed using a small FDM printed plug. The final assembled phantom is displayed in Fig. 4 and a simplified overview of the workflow is presented in Fig. 5.

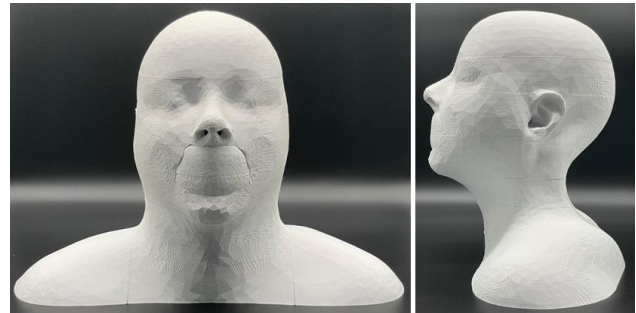


Figure 4: Manufactured head and neck phantom: front view (left), side view (right).

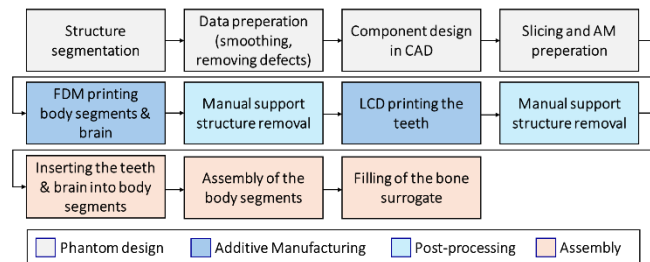


Figure 5: Simplified workflow used for the phantom.

III. Results and discussion

For preliminary validation, we scanned the phantom using a *Somatom go.Open Pro* CT clinical scanner (Siemens Healthcare GmbH, Erlangen, Germany), available in our Radiotherapy Department. For these scans, we selected a head protocol with a tube voltage of 100 kV. This scanner is commonly used for HNC radiation treatment planning. The phantom CT images are depicted in Fig. 6, compared to the reference patient. Further CT images of the phantom are shown in Fig. 7.

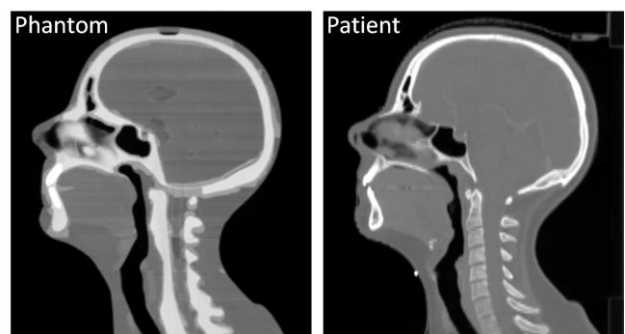


Figure 6: CT images of the head and neck phantom, sagittal view (left), reference patient (right).

The visual assessment of the phantom, when compared to the reference patient used in the design and patient data found in the literature, demonstrated a high level of agreement regarding anatomical features. Key features such as the eyes, brain, teeth, nasal cavities, and esophagus are clearly represented in the images, as shown in Fig. 5.

However, certain simplifications were made in the phantom compared to the actual patient. For instance, the bones were modeled as homogeneous structures for simplicity, meaning there is no differentiation between the periosteum and bone marrow in the phantom.

Additionally, the distances between vertebrae have been simplified, and the bone has been modeled as a continuous structure, which results in the bone appearing thicker, particularly in areas with thinner bone regions (c.f. Fig. 6).

In some areas, the bone surrogate material permeated the PLA, as seen in Fig. 7 (left), resulting in unwanted areas of enhanced contrast near certain bone structures.

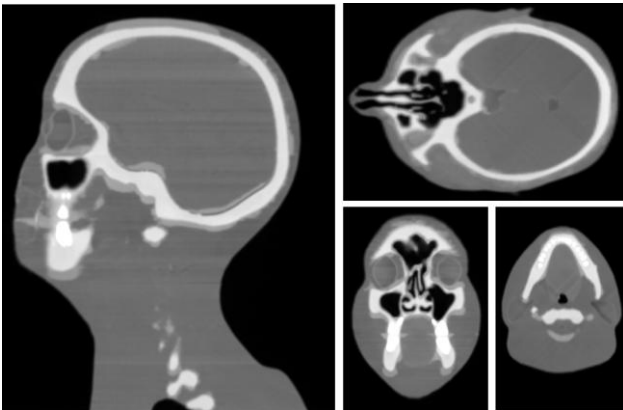


Figure 7: CT images of the head and neck phantom, sagittal view (left), axial view through the nose (top right), coronal view (bottom middle), axial view through the teeth (bottom right).

Moreover, the CT numbers of the different structures were measured using *3D Slicer* [16]. We primarily used the original patient segmentations, which were mapped to the phantom, with the exception of the bone, brain, and body. The measured CT numbers and their standard deviations are listed in Table 1. The desired CT numbers were determined using the reference patient data and additional patient data from the same scanner, along with values found in the literature.

The comparison between the desired CT numbers and the measured CT numbers shows a generally good agreement across the majority of the tissues represented in the phantom, demonstrating that the infill densities chosen for different tissues appear to have a good correlation with their desired CT numbers.

Table 1: Chosen line infill densities for FDM printing of the different structures represented in the phantom, desired CT numbers and the corresponding CT numbers, measured with the clinical CT scanner at a voltage of 100 kV. For bone the results of the surrogate silicone mixture and for teeth the results of the LCD printed mixture are given.

Tissue	Infill (%)	Desired CT numbers (HU)	Mean CT numbers with standard deviation (HU)
Body	83	-10	-14±127
Bone	-	1000	964±65
Brain	87	35	21±153
Cervical esophagus	89	55	35±52
Cricopharyngeal inlet	91	70	72±25
Eye lens L+R	88	40	-30±116
Larynx	90	65	69±98
Lips	87	30	33±121
Liquor	84	0	-68±66
Oral cavity	90	60	60±86
Parotid gland L+R	82	-20	-90±105
Pituitary gland	90	67	65±80
Vitreous body L+R	86	27	4±103
Spinal cord	86	25	29±101
Teeth	-	2700	2638±324
Thyroid gland	100	104	110±42

However, notable discrepancies can be observed in the eye lens, liquor, parotid gland, and vitreous body. These structures exhibit the largest differences in mean CT values as well as a high standard deviation. One reason for this could be that these tissue segmentations were more challenging due to their size and location. The small size of these structures could also have resulted in disproportionately larger air enclosures in the boundary regions between the structures.

The addition of strontium carbonate to the base materials used for manufacturing bone and teeth enabled the CT numbers to reach the desired range of 1000 HU and 2700 HU, demonstrating the effectiveness of this approach in achieving high radiodensity.

IV. Conclusions

During this work, we designed and additively manufactured a physical patient-specific head and neck phantom for CT imaging. Various FDM infill densities were used to represent head and neck organs relevant to CT imaging and radiation treatment of HNC. Teeth were manufactured using an SLA process, while additives in the AM material were used to achieve high HU values. Preliminary analyses of CT imaging showed very good anatomical features and realistic CT numbers.

Future adaptations of the phantom could focus on preventing leakage of the bone surrogate by coating the PLA as well as further adjusting some infill densities to more closely match patient-specific values. Our next steps involve comparing the geometric features of the phantom with the original patient data using the Structural Similarity Index Measurement (SSIM), Dice coefficients, and Hausdorff distances.

In the future, the developed head and neck phantom will serve as a valuable model for multi-center studies, radiomics research, quality assurance, and dose measurements. Its primary purpose is to facilitate the analysis and comparison of imaging data across different CT systems, ensuring consistency and reliability of quantitative analyses in diagnostic imaging. By enabling standardized assessments, the phantom has the potential to enhance clinical diagnostics, support personalized treatment strategies for HNC, and bridge the gap between simulations and testing.

ACKNOWLEDGMENTS

Research funding: The authors state no funding involved.

AUTHOR'S STATEMENT

Conflict of interest: Authors state no conflict of interest.

REFERENCES

- [1] M. Gormley, G. Creaney, A. Schache, K. Ingarfield, and D.I. Conway, Reviewing the epidemiology of head and neck cancer: definitions, trends and risk factors, *British Dental Journal*, vol. 233, 2022, pp. 780-786.
- [2] A. Barsouk, J.S. Aluru, P. Rawla, K. Saginala, and A. Barsouk, Epidemiology, risk factors, and prevention of head and neck squamous cell carcinoma. *Medical Sciences*, vol. 11 (2), 42, 2023.
- [3] S. R. Badiuk, D. K. Sasaki, and D. W. Rickey, An anthropomorphic maxillofacial phantom using 3-dimensional printing, polyurethane rubber and epoxy resin for dental imaging and dosimetry, in *Dento maxillo facial radiology*, vol. 51, 2022.
- [4] M. Grehn, M. Stille, C. Ziemann, F. Cremers, D. Rades, and T. M. Buzug, A New Phantom for Individual Verification of the Dose Distribution in Precision Radiotherapy for Head-and-Neck Cancer, in *Anticancer research*, vol. 39, no. 12, 2019, pp. 6931-6938.
- [5] S. Y. Kim, J. W. Park, J. Park, J. W. Yea, and S. an Oh, Fabrication of 3D printed head phantom using plaster mixed with polylactic acid powder for patient-specific QA in intensity-modulated radiotherapy, in *Scientific reports*, vol. 12, 2022.
- [6] T. Kamomae et al., Three-dimensional printer-generated patient-specific phantom for artificial in vivo dosimetry in radiotherapy quality assurance, in *Physica medica*, vol. 44, 2017, pp. 205-211.
- [7] N. Kadoya et al., Evaluation of a 3D-printed heterogeneous anthropomorphic head and neck phantom for patient-specific quality assurance in intensity-modulated radiation therapy, in *Radiological physics and technology*, vol. 12 (3), 2019, pp. 351-356.
- [8] S. Thrun, D. Pedrosa, M. Schulze, T. M. Buzug, and M. Stille, Creation of a 3D printed human head phantom, in *Transactions on Additive Manufacturing Meets Medicine*, vol. 3 (1), 2021, ID 608.
- [9] J. Schmiech et al., Development of an additively manufactured skull model for the neurointerventional simulator HANNES, in *Transactions on Additive Manufacturing Meets Medicine*, vol. 5 (1), 2023, ID 816.
- [10] M. Wegner, E. Gargioni, and D. Krause, Indirectly additive manufactured deformable bladder model for a pelvic radiotherapy phantom, in *Transactions on Additive Manufacturing Meets Medicine*, vol. 3 (1), 2021, ID 498.
- [11] M. Wegner, and D. Krause, 3D printed phantoms for medical imaging: recent developments and challenges. *Journal of Mechanical Science and Technology*, vol. 38 (9), 2024, pp. 4537-4543.
- [12] M. Wegner, J. Schmiech, E. Sobirey, D. Krause, and E. Gargioni, Requirement analysis in medical phantom development: a survey tool approach with an illustrative example of a multimodal deformable pelvic phantom, in *Frontiers in Physics*, vol. 12, 2024.
- [13] M. Wegner, M. Rosendahl, N. Hinrichsen, D. Krause, and E. Gargioni, Creation and analysis of additive-manufactured CT-equivalent phantom tissue surrogates, in *Transactions on Additive Manufacturing Meets Medicine*, vol. 6 (1), 2024, ID 1785.
- [14] G. Podobnik, P. Strojjan, P. Peterlin, B. Ibragimov, and T. Vrtovec, HaN-Seg: The head and neck organ-at-risk CT and MR segmentation dataset. in *Medical Physics*, vol. 50, 2023, pp. 1917-1927.
- [15] G. Podobnik, HaN-Seg: The head and neck organ-at-risk CT & MR segmentation dataset, Zenodo, 2023.
- [16] A. Fedorov et al., 3D Slicer as an image computing platform for the Quantitative Imaging Network, in *Magnetic Resonance Imaging*, vol. 309, 2012, pp. 1323-1341.